RESEARCH ARTICLE

Toward better understanding vacuum ultraviolet–iodide induced photolysis via hydrogen peroxide formation, iodine species change, and difluoroacetic acid degradation

Yang Yang, Qi Zhang, Baiyang Chen (✉), Liangchen Long, Guan Zhang

State Key Laboratory of Urban Water Resource and Environment, Harbin Institute of Technology (Shenzhen), Shenzhen 518055, China

HIGHLIGHTS

- UV/VUV/I$^-$ induces substantial H$_2$O$_2$ and IO$_3^-$ formation, but UV/I$^-$ does not.
- Increasing DO level in water enhances H$_2$O$_2$ and iodate productions.
- Increasing pH decreases H$_2$O$_2$ and iodate formation and also photo-oxidation.
- The redox potentials of UV/VUV/I$^-$ and UV/VUV changes with pH changes.
- The treatability of the UV/VUV/I$^-$ process was stronger than UV/VUV at pH 11.0.

GRAPHIC ABSTRACT

ARTICLE INFO
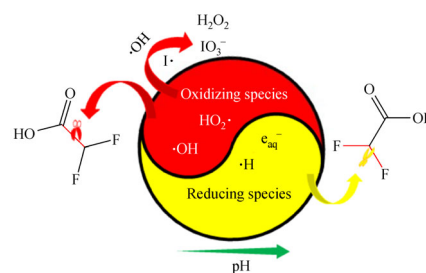
ABSTRACT

Recently, a photochemical process induced by ultraviolet (UV), vacuum UV (VUV), and iodide (I$^-$) has gained attention for its robust potential for contaminant degradation. However, the mechanisms behind this process remain unclear because both oxidizing and reducing reactants are likely generated. To better understand this process, this study examined the evolutions of hydrogen peroxide (H$_2$O$_2$) and iodine species (i.e., iodide, iodate, and triiodide) during the UV/VUV/I$^-$ process under varying pH and dissolved oxygen (DO) conditions. Results show that increasing DO in water enhanced H$_2$O$_2$ and iodate production, suggesting that high DO favors the formation of oxidizing species. In contrast, increasing pH (from 6.0 to 11.0) resulted in lower H$_2$O$_2$ and iodate formation, indicating that there was a decrease of oxidative capacity for the UV/VUV/I$^-$ process. In addition, difluoroacetic acid (DFAA) was used as an exemplar contaminant to verify above observations. Although its degradation kinetics did not follow a constant trend as pH increases, the relative importance of mineralization appeared declining, suggesting that there was a redox transition from an oxidizing environment to a reducing environment as pH rises. The treatability of the UV/VUV/I$^-$ process was stronger than UV/VUV under pH of 11.0, while UV/VUV process presented a better performance at pH lower than 11.0.

1 Introduction

Ultraviolet-based technologies have been studied widely for water pollutant treatment due to high degradation capacity, operational convenience, and low environmental impact (Deng et al., 2013; Alapi et al., 2017; He et al.,

✉ Corresponding author
E-mail: chen.baiyang@hit.edu.cn

2019; Cui et al., 2020; Li et al., 2020; Yang et al., 2020). Among all ultraviolet-induced processes, photolysis via coexisting 254 nm ultraviolet (UV) and 185 nm vacuum ultraviolet (VUV) has gained considerable interests recently because of its ability to generate multiple types of radicals (Eqs. (1) and (2), Table 1) (Gonzalez et al., 2004; Zoschke et al., 2014; Alapi et al., 2017; Chen et al., 2019; Zhang et al., 2020). However, also because of this reason, its inherent mechanisms are hard to elucidate. For example, Gonzalez et al. once reported that UV/VUV process alone is capable of generating at least 13 reactive species (RSs) including •OH, •H, e$_{aq}^-$, HO$_2$•, O$_2$•$^-$, H$_2$, O$_2$, H$_2$O$_2$, HO$_2^-$, H$^+$, OH$^-$, O$_3$•$^-$, and HO$_3$• (Gonzalez et al.,

2004). While some RSs are oxidizing species (Pourakbar et al., 2016; Alapi et al., 2017; Moradi and Moussavi, 2018; Abbaszadeh Haddad et al., 2019), many coexisting RS are reducing species (i.e., e_{aq}^-, •H). Therefore, the roles of oxidizing and reducing species in a UV/VUV process are very difficult to distinguish (Zoschke et al., 2014).

In literature, VUV alone is often regarded as an advanced oxidative process (AOP) because of its ability to produce more •OH than e_{aq}^- (Eqs. (1) and (2)) (Gonzalez et al., 2004; Li et al., 2012). In contrast, photolysis induced by UV and iodide (I$^-$, molar absorptivity coefficient ε_{254} = 220 M^{-1} cm^{-1} (Yu et al., 2018)) is usually considered as a robust advanced reductive process (ARP) because it generates e_{aq}^- that can reduce pollutants like perfluorinated compounds (Qu et al., 2010; Park et al., 2011; Sun et al., 2017a), trihalomethanes (Tobien et al., 2000), haloacetic acid (Li et al., 2014; Wang et al., 2020), and antibiotic drugs (Yang et al., 2018b). However, there are some exceptions; for example, one study once reported that UV/I$^-$ photolysis oxidized arsenic (As (III)) into As (V) via triiodide (I$_3^-$) (Eqs. (3)–(10)) (Yeo and Choi, 2009),

meaning that besides reductive reactants, oxidative species can be generated too during the UV/I$^-$ process. To take advantages of both VUV and UV/I$^-$ processes, two exemplar studies have compared the treatability of UV/VUV/I$^-$ process with other processes for pollutant control (Giri et al., 2014; Gu et al., 2017). In one study, UV/VUV/I$^-$ performed better in removing perfluorooctane sulfonate than UV/VUV/persulfate under ambient conditions; however, adjusting dissolved oxygen (DO) and pH switched their relative effectiveness (Gu et al., 2017). In another study, the degradation kinetics of perfluorooctanoic acid (PFOA) were ranked as UV/VUV>UV/VUV/I$^-$>UV/I$^-$ under selected experimental conditions (Giri et al., 2014). This is somehow unexpected because PFOA is often more vulnerable to reducing agent than oxidizing species. Note that the effects of experimental conditions (i.e., DO and pH) were not evaluated (Giri et al., 2014). Thus, a better understanding of the mechanisms behind the UV/VUV/I$^-$ process and a systematic comparison between UV/VUV and UV/VUV/I$^-$ are necessary.

Of note, the reactive species produced by UV/VUV and

Table 1 A summary of photochemical equations and rate constants involved in this study.

Equations	Rate constants	Ref.
(1) $H_2O + hv_{185} \rightarrow$ •OH + •H	$\Phi_{•OH} = 0.33$	Gonzalez et al., 2004
(2) $H_2O + hv_{185} \rightarrow$ •OH + H$^+$ + e_{aq}^-	$\Phi e_{aq}^- = 0.045$	Gonzalez et al., 2004
(3) I$^-$ + H$_2$O + $hv_{254} \rightarrow$ I$^-$H$_2$O*		Yeo and Choi, 2009
(4) I$^-$H$_2$O* $\rightarrow$ (I•, e$^-$) + H$_2$O		Yeo and Choi, 2009
(5) (I•, e$^-$) $\rightarrow$ I• + e_{aq}^-	$\Phi e_{aq}^- = 0.3–0.4$	Qu et al., 2010
(6) (I•, e$^-$) + O$_2$ $\rightarrow$ I• + O$_2$•$^-$		Yeo and Choi, 2009
(7) I• + I• $\rightarrow$ I$_2$	$k_7 = 1.0 \times 10^{10}$ M^{-1} s^{-1}	Yeo and Choi, 2009
(8) I• + I$^-$ $\leftrightarrow$ I$_2^-$	$k_8 > 1.2 \times 10^4$ M^{-1} s^{-1}	Yeo and Choi, 2009
(9) I$_2^-$ + I$_2^-$ $\rightarrow$ I$_3^-$ + I$^-$	$k_9 = 3.2 \times 10^9$ M^{-1} s^{-1}	Yeo and Choi, 2009
(10) I$_2$ + I$^-$ $\leftrightarrow$ I$_3^-$	$k_{10} = 700$ M^{-1} s^{-1}	Yeo and Choi, 2009
(11) $H_2O_2 \leftrightarrow$ H$^+$ + HO$_2^-$	pK$_a$ = 11.6	Song et al., 2017
(12) •OH $\leftrightarrow$ H$^+$ + •O$^-$	pK$_a$ = 11.9	Nosaka and Nosaka, 2017
(13) HO$_2$• $\leftrightarrow$ H$^+$ + O$_2$•$^-$	pK$_a$ = 4.8	Nosaka and Nosaka, 2017
(14) •H $\leftrightarrow$ H$^+$ + e_{aq}^-	pK$_a$ = 9.7	Nosaka and Nosaka, 2017
(15) HO$_3$• $\leftrightarrow$ H$^+$ + O$_3$•$^-$	pK$_a$ = 8.2	Nosaka and Nosaka, 2017
(16) e_{aq}^- + H$^+$ $\rightarrow$ •H	$k_{16} = 2.3 \times 10^{10}$ M^{-1} s^{-1}	Cui et al., 2020
(17) e_{aq}^- + •H + H$_2$O $\rightarrow$ H$_2$ + OH$^-$	$k_{17} = 3.0 \times 10^{10}$ M^{-1} s^{-1}	Cui et al., 2020
(18) e_{aq}^- + O$_2$ $\rightarrow$ O$_2$•$^-$	$k_{18} = 1.9 \times 10^{10}$ M^{-1} s^{-1}	Cui et al., 2020
(19) e_{aq}^- + O$_2$•$^-$ $\rightarrow$ O$_2^-$	$k_{19} = 1.3 \times 10^{10}$ M^{-1} s^{-1}	Cui et al., 2020
(20) HOI + HOI $\rightarrow$ IO$_2^-$ + I$^-$ + H$^+$		Sun et al., 2017a
(21) HOI + OI$^-$ $\rightarrow$ IO$_2^-$ + I$^-$ + H$^+$		Sun et al., 2017a
(22) HOI + IO$_2^-$ $\rightarrow$ IO$_3^-$ + I$^-$ + H$^+$		Sun et al., 2017a
(23) e_{aq}^- + I$_3^-$ $\rightarrow$ I$_2$•$^-$ + I$^-$		Sun et al., 2017a
(24) •OH + •OH $\rightarrow$ H$_2$O$_2$	$k_{24} = 4.0 \times 10^9$ M^{-1} s^{-1}	Zhang et al., 2020
(25) •H + O$_2$ $\rightarrow$ HO$_2$•	$k_{25} = 1.0 \times 10^{10}$ M^{-1} s^{-1}	Moussavi and Rezaei, 2017
(26) 2HO$_2$• $\rightarrow$ H$_2$O$_2$ + O$_2$	$k_{26} = 2.0 \times 10^{10}$ M^{-1} s^{-1}	Moussavi and Rezaei, 2017

UV/VUV/I$^-$ processes (H$_2$O$_2$, HO$_2$•, •H, •OH, and HO$_3$•) can be deprotonated to form HO$_2^-$, O$_2$•$^-$, e$_{aq}^-$, •O$^-$, and O$_3$•$^-$ when the solution pH exceeds their acidic dissociation coefficients (pK$_a$) (Eqs. (11)–(15)), meaning that different species dominate at different pH (Roth and LaVerne, 2011; Nosaka and Nosaka, 2017). If pH is adjusted to a certain level that minimizes e$_{aq}^-$ formation (Eqs. (16) and (17)) (Buxton et al., 1988), the oxidizing species likely dominate the oxidating-reducing system. Since H$_2$O$_2$ formation is mainly attributed to •OH recombination, the appearance of H$_2$O$_2$ is likely an indicator of the presence of •OH (Diesen and Jonsson, 2014). Besides, H$_2$O$_2$ is more stable and its detection is more convenient than •OH detection. Therefore, we intend to monitor the evolutions of H$_2$O$_2$ under varying environmental conditions to better understand the UV/VUV and UV/VUV/I$^-$ processes.

To our best knowledge, there is no systematic study on the UV/VUV/I$^-$ induced photolysis so far. Consequently, we carried out some experiments to testify the presence of oxidizing/reducing species. First, we checked the roles of UV and VUV irradiation on the H$_2$O$_2$ formation and iodine species (i.e., I$^-$, IO$_3^-$, and I$_3^-$) evolution. Then, we assessed the impacts of water pH and DO on the evolutions of H$_2$O$_2$ and iodine species along UV/VUV/I$^-$ process. Lastly, we verified the oxidizing/reducing capacity of UV/VUV/I$^-$ process by degrading a typical compound (difluoroacetic acid, DFAA).

2   Materials and methods

2.1   Chemicals and reagents

Sodium hydroxide, sodium iodide, sodium fluoride, potassium iodate, and acetic acid were purchased from Aladdin Co. Ltd. in the form of powder (>99.0% purity). DFAA (>97.0% purity) was obtained from Adamas-beta Inc. The stock solution of H$_2$O$_2$ was made using a commercial H$_2$O$_2$ product (30.0% concentration) purchased from Xilong Scientific Inc. All solutions were prepared using ultrapure water with an electric resistance of 18.2 MΩ.

2.2   Photoreactor and operation procedure

All photolysis experiments were performed in duplicate using a stainless-steel, horizontally-placed batch reactor with a volume of 450 mL (Fig. S1). Two types of low-pressure mercury lamp were used: one emitting both 185 nm and 254 nm wavelengths of light (henceforth referred to as a UV/VUV lamp), and one emitting only 254 nm wavelength light (UV lamp). Both lamps were 15 mm in diameter, 212 mm in length, 8 W in power output, and purchased from the same manufacturer (Uvcn Inc., China). In each experiment, a quartz tube was placed in the reactor and then a lamp was placed inside the tube.

The initial concentrations of I$^-$ were fixed at 1.0 mg/L, and DFAA at 10.0 mg/L unless otherwise stated. Although it may not reflect well their concentrations in typical waters (the average I$^-$ concentration in sea was 0.06 mg/L and DFAA was not more than 3.1 × 10^{-5} mg/L in the lakes (Scott et al., 2002)), DFAA is used mainly to characterize the mechanism rather than to evaluate the treatability of the process. Prior to photolysis, lamps were warmed up for 30 min to ensure the stability of photon flux. During experiments, reactors were oscillated on a shaking table to maintain a homogeneous solution. During time intervals, 8.0 mL of sample was retrieved each time from the outlet of the reactor with pipet and analyzed. All experiments were conducted in an air-conditioned room with a temperature of 20°C.

The photonic intensity of 254 nm UV emitted from the UV/VUV lamp was similar to that emitted from the UV lamp, which was confirmed by using a UV radiation meter equipped with a 254 nm detector (Beijing Shida photo-electric technology Co., Ltd, China). The detailed methods for determining photoreactor incident fluence and optical path were described in previous studies (Wang et al., 2017; Zhang et al., 2020). Briefly, the photon flux was measured as 0.653 μEinstein/s for the 185 nm VUV by photolysis of deionized water. The photon flux was estimated as 14.6 μEinstein/s for the 254 nm UV by photolysis of 55 mM of H$_2$O$_2$. In addition, the optical path length inside the solution of the UV lamp was determined to be 1.37 cm by photodegrading a solution containing 0.1 mmol/L of H$_2$O$_2$.

2.3   Analytical methods

The concentrations of H$_2$O$_2$, IO$_3^-$, DFAA, fluoride, and acetic acid were all determined using an ion chromatograph (IC-2010 Tosoh, Japan) equipped with a Thermo-fisher AS15 column (150 mm × 3 mm, 20 mmol/L aqueous solution of KOH as eluent, flow rate at 0.5 mL/min, and column temperate at 30°C) and an ultraviolet detector at a wavelength of 210 nm. H$_2$O$_2$ detection was accomplished using the method described in detail by Song et al. (Song et al., 2017) with one improvement. That is, the method detection limit (MDL) of H$_2$O$_2$ was lowered to 3.0 μg/L in this study because of the reduced baseline signal and enlarged sample injection volume (500 vs. 100 μL).

The concentrations of I$^-$ were measured by another ion chromatography equipped with a different column (i.e., SH-AC-17, 250 mm × 4.6 mm, Shine, China) and an ultraviolet detector at a characteristic wavelength of 226 nm. The purpose of applying different IC columns was to reduce the elution time of I$^-$. The operational conditions were set as following: 10.0 mmol/L KOH as eluent, flow rate at 0.8 mL/min, and column temperate at 35°C.

The mineralization level of DFAA was estimated by total

organic carbon (TOC), which was determined by a TOC analyzer (TOC-L$_{CPH}$, Shimadzu, Japan) with an MDL of 0.1 mg-C/L. pH measurement was carried out using a calibrated pH electrode (Orion 8103BN, Thermo Scientific). The pH of test solutions was adjusted by spiking NaOH without using buffer to avoid introduction of interfering compounds into the water since carbonate/ bicarbonate and phosphate buffers can decrease the formation of H_2O_2 during UV/VUV process (Li et al., 2021). Fig. S2 demonstrates some pH changes along the UV/VUV/I$^-$ process. As seen, although the solution pH during the UV/VUV/I$^-$ process change moderately for water with initial pH of 8.2, the average pH of this process was markedly different from other two waters containing initial pH of 9.9 and 6.2. So, the results obtained from solutions without using buffer were still trustworthy to reflect the differences of reactions in these solutions. Initial DO concentration was measured using a polarographic oxygen probe (Ohaus Inc., USA) calibrated in air, which has a DO of approximately 8.5 mg/L at 25°C, and a solution saturated with sodium sulfite, which has a DO of zero (Yang and Jonsson, 2014). The sensitivity of DO meter is 0.1% with a resolution of 0.01 mg/L. Prior to photolysis, the initial DO level was adjusted by bubbling

nitrogen gas (N_2) into the solution; during experiments, the DO level was maintained by purging N_2 on the surface of water.

3   Results and discussion

3.1   The distinctive roles of VUV and UV

To distinguish the roles of VUV and UV wavelengths during UV/VUV/I$^-$ process, a background study was first performed by comparing the potentials of H_2O_2 formation and I$^-$ transformation between UV and UV/VUV lamps. Figures 1(a) and 1(b) show that both H_2O_2 and IO_3^- concentrations increased dramatically by irradiating an I$^-$-containing water under a UV/VUV lamp; in contrast, little H_2O_2 and IO_3^- were generated under a UV lamp. Because IO_3^- is one of the oxidation products and can stay steadily in the system, the appearance of IO_3^- might serve as another indicator for the occurrence of oxidative species. This finding confirms that the formation of H_2O_2 and IO_3^- can be primarily attributed to the 185 nm wavelength VUV emitted by the UV/VUV lamp. Although VUV often accounts for only a small portion (4.3%) of total light
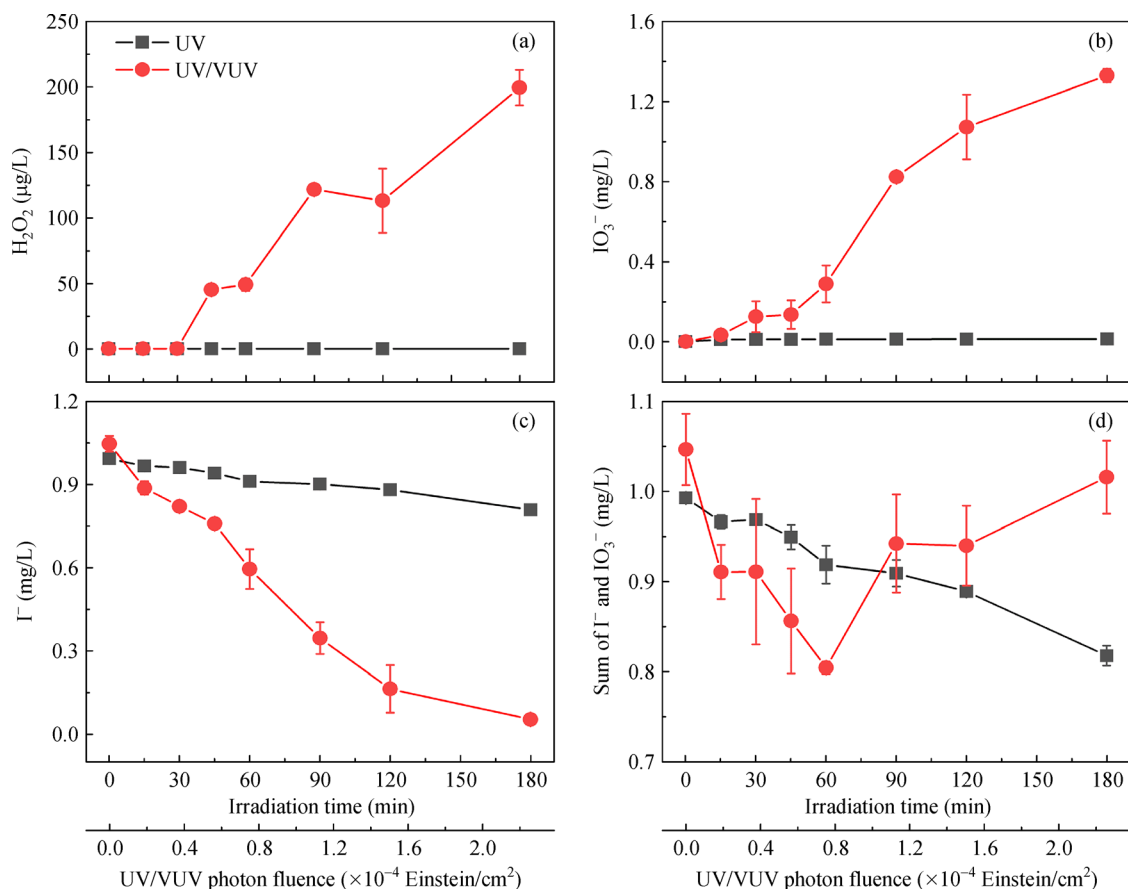
Fig. 1 A comparison of H_2O_2 formation and iodine species evolution between UV and UV/VUV photolysis processes ([I$^-$]$_0$ = 1.0 mg/L, DO = 8.5 mg/L, initial pH = 6.0 with no buffer used).

emitted by a UV/VUV lamp (Yang et al., 2018a), VUV actually plays the key role in generating radicals, H_2O_2, and IO_3^-.

The concentrations of I^- decreased with the duration of irradiation (Fig. 1(c)). The sums of I^- and IO_3^- decreased in both UV and UV/VUV irradiation processes at the beginning. However, the sums of I^- and IO_3^- contents returned to initial I^- dosages at the end of UV/VUV irradiation process (Fig. 1(d)). This observation indicates that certain iodine-containing intermediates were formed in the middle of the process. For example, self-reaction of hypoiodous acid may occur and generate polyiodide during UV photolysis of I^- (Sun et al., 2017a). According to Eqs. (7)–(9), the decrease of I^- is partially due to the generation of I_3^- which can be measured by its characteristic UV absorption peak (i.e., 285 nm) (Wei et al., 2005). To support this hypothesis, we measured the absorption spectra of a solution containing 10.0 mg/L of I^- during UV/VUV irradiation. Fig. S3 shows that the peak associated with I^- (λ = 226 nm) declined over time, while the peak associated with I_3^- at λ of 285 nm kept increasing, meaning that I_3^- was formed continuously as an intermediate product. According to its molar absorption coefficient (3.5×10^4 L/mol-cm at 285 nm) (Wei et al., 2005), the maximum concentration of I_3^- reached 0.2 mg-I/L, compensating for the I^- loss to some degree. Notably, the UV absorbances from 300 nm to 500 nm also increased, suggesting that other I-containing intermediates (e.g., hypoiodite and iodite) might have been formed too. In literature, it was reported that hypoiodite can react with hypoiodous acid to form iodite, which then forms IO_3^- and I^- (Eqs. (20)–(22)). When I_3^- reacted with $\cdot H/e_{aq}^-$ (Eq. (23)) and generated I^-, it increased the total levels of I^- and IO_3^- in the end. In contrast, the UV/I^- process generated iodine species (i.e., I_3^-, HOI, and I_2), which may consume I^-, thus leading to I^- loss (Sun et al., 2017a).

To further verify the impacts of VUV and UV irradiation on the changes in concentrations of iodine species, a solution dosed with I^- was irradiated first using UV/VUV wavelengths for 60 min and then using the UV wavelength alone for another 60 min. As seen in Fig. S4, the I^- levels decreased substantially during the initial UV/VUV irradiation period, but increased back to initial levels during the UV irradiation period. This indicates that VUV irradiation of water has transformed I^- into other iodine species, probably via the action of oxidizing radicals, whereas UV irradiation has transformed those iodine species back into I^- through reactions with certain reducing agents (Zhang et al., 2016). Increasing pH reduced the transformation of I^- during the VUV process, which is consistent with the fact that $\cdot OH$ is less effective under alkaline conditions (Deng et al., 2013).

3.2 Effects of dissolved oxygen

As shown in Fig. 2(a), H_2O_2 concentrations in a high DO

solution increased continually through the irradiation process, with the maximum concentration reaching 199.09 μg/L at the end, whereas the maximum H_2O_2 concentration in a low DO solution was only 36.14 μg/L. This result indicates that increasing DO content enhanced H_2O_2 generation during the UV/VUV/I^- process. This finding is inconsistent with an earlier study that H_2O_2 was mostly formed through an oxygen-independent $\cdot OH$ recombination process during VUV irradiation, perhaps because the earlier study did not add any ions (Yang et al., 2018a). Because the rate constant of reaction between $\cdot OH$ and I^- ($k = 1.1 \times 10^{10}$ M^{-1} s^{-1} (Motohashi and Saito, 1993)) is faster than that of $\cdot OH$ self-combination ($k = 4.0 \times 10^9$ M^{-1} s^{-1}, Eq. (24)), the discrepancies between studies are probably caused by the presence of I^-. In addition, the dominant reducing radical under the experimental conditions (Eq. (14)) is $\cdot H$, which may promote H_2O_2 formation by forming an oxidizing species ($HO_2\cdot$) in a high DO solution (Eqs. (25) and (26)) (Moussavi and Rezaei, 2017).

Regarding I^- evolution, both IO_3^- generation and I^- transformation kinetics in the high DO (Fig. 2(b)) solution were higher than those in the low DO solution (Fig. 2(c)). This is probably because reducing radicals ($\cdot H/e_{aq}^-$) can be consumed by oxygen in a high DO solution (Eqs. (18) and (19)), and therefore I^- was better oxidized under these conditions than that in a low DO solution. In literature, purging N_2 is conducive to increase photon fluence rate as the photon fluence rates increased with N_2 purging rate (Meunier et al., 2016). So, the increased photon fluence rate may contribute to IO_3^- generation under the low DO solution. Interestingly, the sums of I^- and IO_3^- declined first but returned to initial levels in high DO water (Fig. 2(d)), suggesting that some iodine-containing intermediates (such as $I\cdot$) were formed and then oxidized to IO_3^- under high DO conditions. In contrast, the sum concentrations of I^- and IO_3^- present an ever-decreasing trend in the low DO solution. Figure S5 documented the DO changes during UV/VUV/I^- process at different initial DO levels. The DO consumed in high DO solution was higher than that in low DO solution. This suggests that the losses of I^- and IO_3^- in low DO solution are caused by the inhibited generation of $I\cdot$ (Eq. (6)) and subsequently inhibitive effect on formation of I_2 (Eq. (7)) and HOI (I_2 hydrolysis). It suggests that although adjusting DO to a low level can reduce some side reactions (Sun et al., 2017a), it may cause I^- loss and increase other iodine-containing intermediates' generation.

3.3 Effects of pH

Water pH is another key factor that can influence the evolution and reactivity of radicals (Cui et al., 2020); therefore, its impact on UV/VUV/I^- process is of interest. Figure 3(a) shows the time profile of H_2O_2 production under varying initial pH conditions during the UV/VUV/I^- process. Production of H_2O_2 decreased from 199.1 to
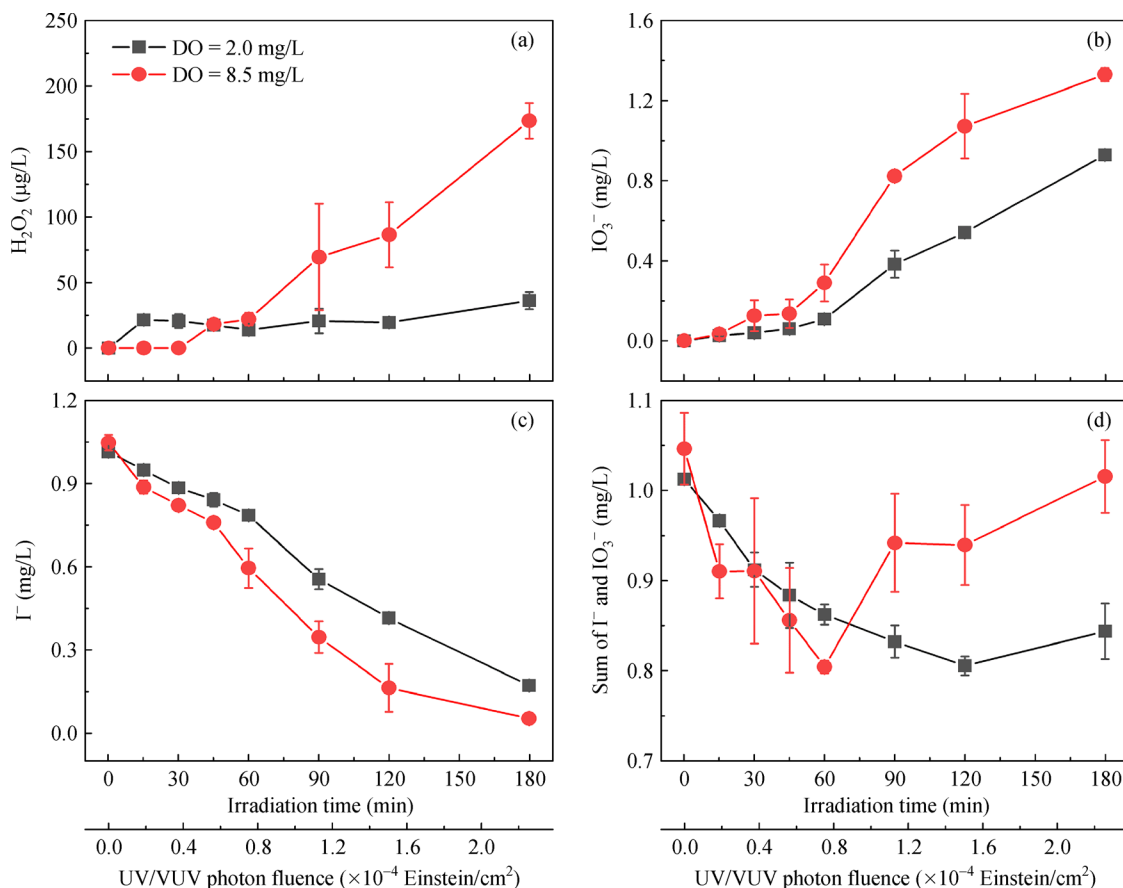
Fig. 2 Effects of DO on H_2O_2 formation and iodine species evolution during UV/VUV photolysis ($[I^-]_0 = 1.0$ mg/L, initial pH = 6.0 with no buffer used).

128.8 μg/L as pH increased from 6.0 to 8.0, and became undetectable when pH increased further to 10.0. Similarly, IO_3^- generation and I^- transformation levels decreased with rising pH (Figs. 3(b) and 3(c)). Since the rate constant of reaction between •OH and I^- ($k = 1.1 \times 10^{10}$ M^{-1} s^{-1}) is approximate to that of hydroxide (OH^-) and •OH ($k = 1.2 \times 10^{10}$ M^{-1} s^{-1}) (Wang et al., 2020), the reaction between I^- and •OH can reasonably be inhibited by rising pH. At pH levels of 6.0 and 8.0, OH^- concentrations were much lower than I^- concentrations; hence, •OH reacts mainly with I^-, consequently increasing production of IO_3^-. However, when solution pH increased to 10.0 and the concentration of OH^- surpassed the concentration of I^-, •OH primarily reacted with OH^- resulting in decreases in the formation of H_2O_2 and IO_3^-. Figure S6 shows a strong correlation between H_2O_2 and IO_3^- formation levels during the UV/VUV/I^- process, suggesting that their formations are caused by the same oxidizer. In addition, it is noteworthy that IO_3^- generation begins earlier than H_2O_2 formation, which is mainly because the concentration of I^- was much higher than that of •OH generated in the system.

As shown in Fig. 3(d), at pH levels of 6.0 and 8.0, the sums of I^- and IO_3^- concentrations generally decreased in the early stage and then returned to initial levels; at pH of

10.0, however, concentrations of iodine species remained stable. This indicates that the concentration of •OH was too low under high pH conditions to oxidize I^- into IO_3^-, which is consistent with the result (shown in Fig. S4) that increasing pH reduced the transformation of I^-. In addition, the sums of I^- and IO_3^- tend to exhibit a stable trend with the increases of solution pH, meaning that the generation of iodine-containing intermediates was negligible at high pH solution. Therefore, although iodine species may quench •H/e_{aq}^- (Buxton et al., 1988), the low I^- concentration (1.0 mg/L) had a negligible effect on e_{aq}^- at high pH solution. Figure 4 presents a schematic diagram of H_2O_2 formation and IO_3^- evolution during the UV/VUV/I^- process under varying DO and pH conditions, which summarizes the findings mentioned above.

3.4 DFAA degradation by the UV/VUV/I^- process

To better understanding the inner mechanism of UV/VUV and UV/VUV/I^- processes, we selected DFAA as an exemplar compound since it is known to be vulnerable to both oxidizing and reducing species (Scott et al., 2002; Dorgerloh et al., 2019). Figure S7 shows the DFAA kinetics of degradation, mineralization, and defluorination
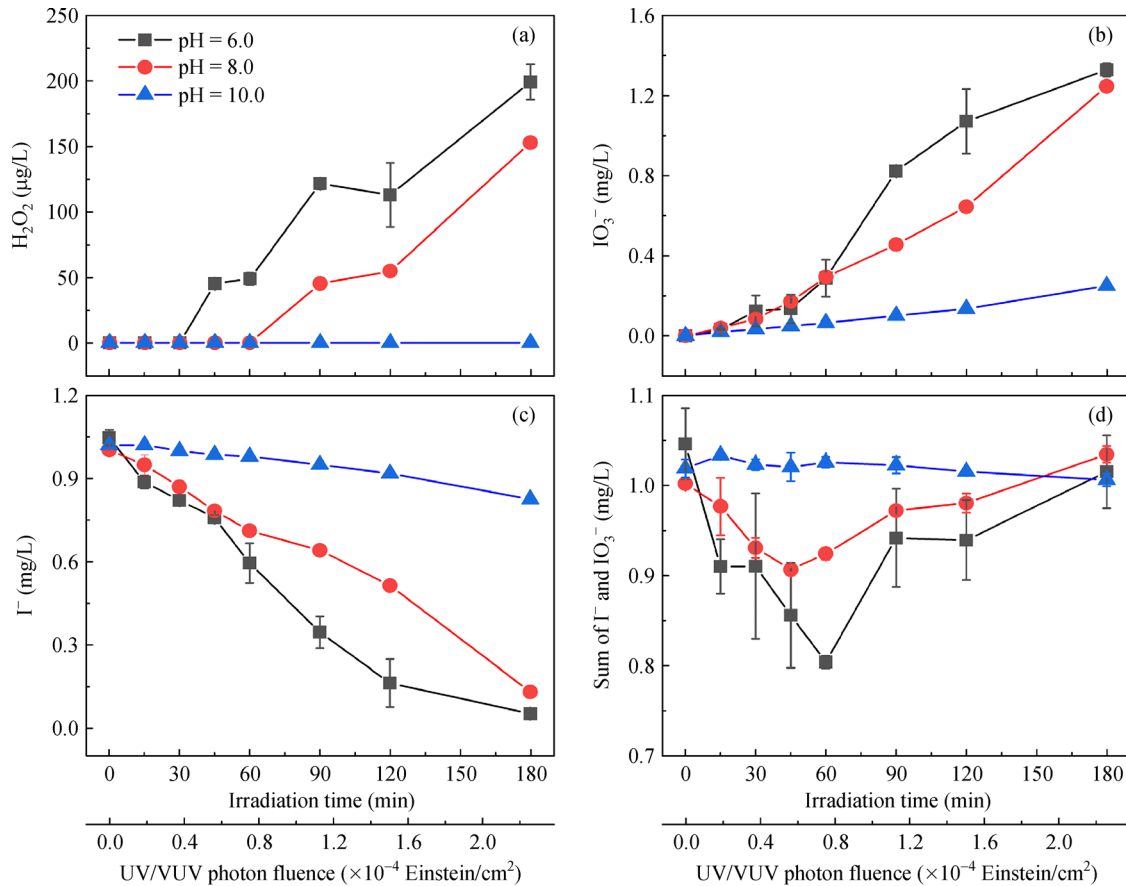
Fig. 3 Effects of pH on H_2O_2 formation and iodine evolution during UV/VUV photolysis ($[I^-]_0 = 1.0$ mg/L, DO = 8.5 mg/L with no buffer used).
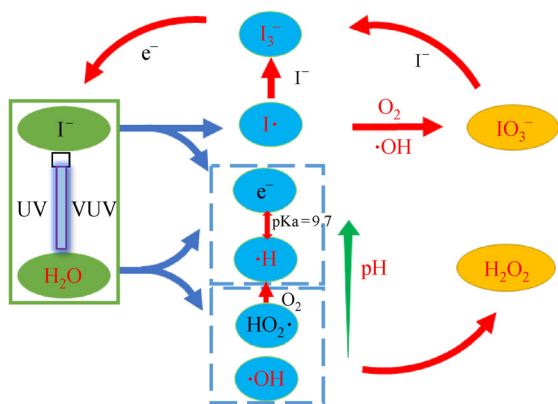

Fig. 4 A schematic of H_2O_2 formation and iodine species evolution during the UV/VUV/I$^-$ process.

under varying pH conditions during the UV/VUV/I$^-$ process. These reactions generally followed first-order reaction kinetics well, with correlation coefficients (R^2) being $\geqslant 0.94$. Figure 5(a) shows that the largest DFAA degradation rate constant (k_d) appeared at pH of 9.0, followed by pH of 6.0, 10.0, 8.0, and 11.0, meaning that the rates of DFAA degradation first increased but

decreased later with pH increases. The favorable pH (i.e., 9.0) is quite different from other UV-induced AOPs (e.g., UV/H_2O_2, UV/persulfate, UV/chlorine, UV/peroxymono-sulfate, etc.), which usually favor pH below 7.0 (Deng et al., 2013; Wang et al., 2016). Further increasing pH from 9.0 did not enhance the degradation ability of UV/VUV/I$^-$ process either, which is also different from most of UV-induced ARPs (e.g., UV/I$^-$, UV/sulfite, UV/sulfide, UV/dithionite, UV/ferrous, etc.) (Liu et al., 2013; Liu et al., 2014; Sun et al., 2017b; Xie et al., 2017), which usually increase with rising pH. The highest rate of DFAA mineralization (k_m) was found at pH of 6.0, followed by pH of 9.0, 10.0, 8.0, and 11.0, which generally presents a decreasing trend with the pH rises although the trend is not so consistent. As for k_d, the rate (k_f) followed a pattern similar to DFAA degradation, i.e., pH 9.0>6.0>10.0>8.0>11.0, suggesting that the DFAA degradation was mainly driven by defluorination process.

Because direct photolysis, photo-oxidation, and photo-reduction can all contribute to the degradation of DFAA, it is of interest to understand their contributions. In theory, direct photolysis and photo-oxidation together may con-tribute to mineralization and defluorination via cleavages of C-C and C-F bonds (Vicente et al., 1994; Fan X et al.,
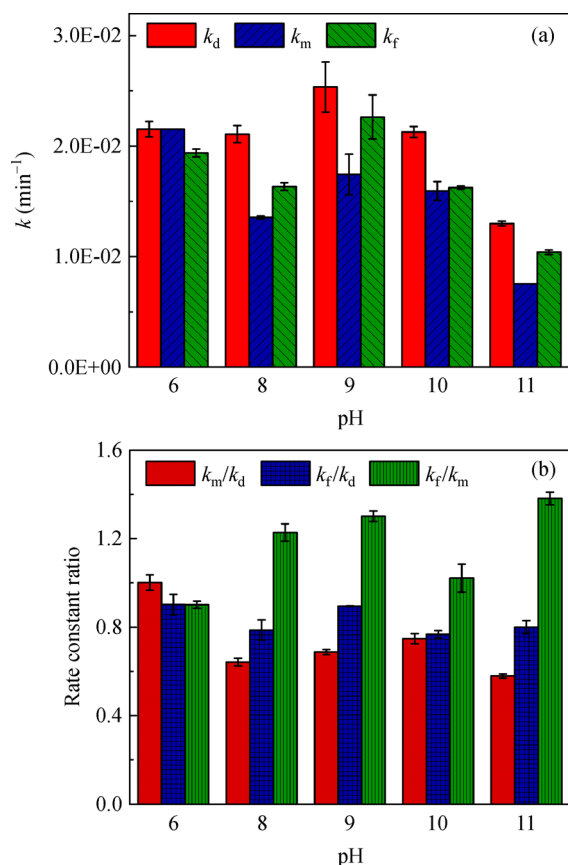
Fig. 5 Effects of pH on the rate constants of degradation (k_d), mineralization (k_m), and defluorination (k_f) of DFAA (a) and the ratio changes of k_m/k_d, k_f/k_d, and k_f/k_m (b) ([I^-]$_0$ = 1.0 mg/L, DO = 8.5 mg/L with no buffer used).

2015; Gorka and Schnermann, 2016), while direct photolysis and photo-reduction together may contribute to defluorination via cleavage of C-F bonds (Giri et al., 2014; Liu et al., 2021). To verify the presence of photoreduction process, we checked the intermediates during UVVUV/I^- process at pH of 9.0 (Fig. S8), and found that acetic acid was indeed formed (1.34 mg/L in maximum at 30 min), indicating that there was cleavage of C-F bonds present in this study. Therefore, we attempted to identify the trends by monitoring the changes in the ratios of k_m to k_d, k_f to k_d, and k_f to k_m. As shown in Fig. 5(b), the k_m/k_d ratios generally decreased (from 1.0 to 0.6), k_f/k_m ratios increased (from 0.9 to 1.4), and k_f/k_d ratios maintained stable (0.8±0.1) along the increases of pH from 6.0 to 11.0. These results indicate that the contribution of mineralization to DFAA degradation (i.e., k_m/k_d, a symbol of photo-oxidation) is higher than the contribution of defluorination (i.e., k_f/k_d, a symbol of photo-reduction) under low pH conditions, while their relative importance was reversed under high pH conditions. These observations in DFAA transformation are consistent with the trends of H_2O_2 and IO_3^- formation (Fig. 3), suggesting that

the oxidative capacity of UV/VUV/I^- was weakened while its reductive ability increased along the pH increases.

In addition, we conducted UV/VUV photolysis tests without adding I^- as a comparison for DFAA degradation, mineralization, and defluorination under varying pH (Fig. S9). In general, the UV/VUV process was more robust in DFAA degradation than the UV/VUV/I^- process under most of pH conditions. However, the k_d, k_m, and k_f at pH of 11.0 for the UV/VUV/I^- process were higher than those for the UV/VUV photolysis. This indicates that the degradation efficiency of UV/VUV is not always better than UV/VUV/I^- under all conditions. The best performance of the UV/VUV process was found at pH of 10.0, higher than 9.0 as found for the UV/VUV/I^- process. It suggests that the addition of I^- had lowered the pH threshold of photoreduction probably because of the increase of e_{aq}^- yields. Overall, both UV/VUV and UV/VUV/I^- processes seemed to undergo a similar redox transition as pH rises.

4 Conclusions

Our results contribute to better understanding the mechanisms behind the UV/VUV/I^- process by providing evidences of changes in the iodine species and H_2O_2. We investigated several factors affecting the iodine speciation and H_2O_2 formation, including the roles of light wavelengths (VUV vs. UV), DO levels, and solution pH. In addition, we have compared the DFAA degradation efficiencies between UV/VUV and UV/VUV/I^- process at a range of pH. The key findings are identified as follows:

1) Most of H_2O_2 and IO_3^- formed by the UV/VUV/I^- process were ascribed to VUV oxidation alone. The conversion from I^- to IO_3^- may involve several steps, resulting in formation of at least one intermediate product, I_3^-.

2) Higher H_2O_2 and IO_3^- formation were observed in high DO water than those in low DO water, probably because reducing species ($\cdot H/e_{aq}^-$) can be consumed by DO to promote H_2O_2 yields, which subsequently enabled oxidation of more I^- into IO_3^- by $\cdot OH$.

3) Water pH is another key factor controlling the oxidative potentials of the UV/VUV/I^- process. Increasing pH from 6.0 to 11.0 reduced H_2O_2 and IO_3^- formation significantly and shifted the DFAA's photodegradation from mineralization to dehalogenation.

4) UV/VUV process had better performance than UV/VUV/I^- process in degrading DFAA under most of pH conditions except for pH of 11.0. The addition of I^- may enhance the photo-reducing capacity of the UV/VUV process to some degree; however, addition of I^- is also inhibitive to light usage, thus presenting a trend of initial drop followed by increase with rising pH in the DFAA degradation rate for the UV/VUV/I^- process.

References

Abbaszadeh Haddad F, Moussavi G, Moradi M (2019). Advanced oxidation of formaldehyde in aqueous solution using the chemical-less UVC/VUV process: Kinetics and mechanism evaluation. Journal of Water Process Engineering, 27: 120–125

Alapi T, Schrantz K, Arany E, Kozmér Z (2017). Advanced Oxidation Processes for Water Treatment: Fundamentals and Applications. London: IWA Publishing

Buxton G V, Greenstock C L, Helman W P, Ross A B (1988). Critical Review of rate constants for reactions of hydrated electrons, hydrogen atoms and hydroxyl radicals ($\cdot$OH/$\cdot$O$^-$) in aqueous solution. Journal of Physical and Chemical Reference Data, 17(2): 513–886

Chen Y, Wang J, Chen B, Wang L (2019). A green and robust method to measure nanomolar dissolved organic nitrogen (DON) by vacuum ultraviolet. Chemical Engineering Journal, 363: 57–63

Cui J, Gao P, Deng Y (2020). Destruction of per- and polyfluoroalkyl substances (PFAS) with advanced reduction processes (ARPs): A critical review. Environmental Science and Technology, 54(7): 3752–3766

Deng J, Shao Y S, Gao N Y, Xia S J, Tan C Q, Zhou S Q, Hu X H (2013). Degradation of the antiepileptic drug carbamazepine upon different UV-based advanced oxidation processes in water. Chemical Engineering Journal, 222: 150–158

Diesen V, Jonsson M (2014). Formation of H$_2$O$_2$ in TiO$_2$ photocatalysis of oxygenated and deoxygenated aqueous systems: A probe for photocatalytically produced hydroxyl radicals. Journal of Physical Chemistry C, 118(19): 10083–10087

Dorgerloh U, Becker R, Kaiser M (2019). Evidence for the formation of difluoroacetic acid in chlorofluorocarbon-contaminated ground water. Molecules (Basel, Switzerland), 24(6): 1039–1045

Fan X, Tao Y, Wei D, Zhang X, Lei Y, Noguchi H (2015). Removal of organic matter and disinfection by-products precursors in a hybrid process combining ozonation with ceramic membrane ultrafiltration. Frontiers of Environmental Science & Engineering, 9(1): 112–120

Giri R R, Ozaki H, Guo X, Takanami R, Taniguchi S (2014). Oxidative-reductive photodecomposition of perfluorooctanoic acid in water. International Journal of Environmental Science and Technology, 11(5): 1277–1284

Gonzalez M G, Oliveros E, Worner M, Braun A M (2004). Vacuum-ultraviolet photolysis of aqueous reaction systems. Journal of Photochemistry and Photobiology C, Photochemistry Reviews, 5(3): 225–246

Gorka A P, Schnermann M J (2016). Harnessing cyanine photooxidation: From slowing photobleaching to near-IR uncaging. Current Opinion in Chemical Biology, 33: 117–125

Gu Y, Liu T, Wang H, Han H, Dong W (2017). Hydrated electron based decomposition of perfluorooctane sulfonate (PFOS) in the VUV/sulfite system. The Science of the Total Environment, 607–608: 541–548

He D, Yang Y, Tang J, Zhou K, Chen W, Chen Y, Dong Z (2019). Synergistic effect of TiO$_2$-CuWO$_4$ on the photocatalytic degradation of atrazine. Environmental Science and Pollution Research International, 26(12): 12359–12367

Li J, Zhang Q, Chen B, Wang L, Zhu R, Yang J (2021). Hydrogen peroxide formation in water during the VUV/UV irradiation process: Impacts and mechanisms of selected anions. Environmental Research, 195: 110751

Li X, Fang J, Liu G, Zhang S, Pan B, Ma J (2014). Kinetics and efficiency of the hydrated electron-induced dehalogenation by the sulfite/UV process. Water Research, 62: 220–228

Liu X, Vellanki B P, Batchelor B, Abdel-Wahab A (2014). Degradation of 1,2-dichloroethane with advanced reduction processes (ARPs): Effects of process variables and mechanisms. Chemical Engineering Journal, 237: 300–307

Liu X, Yoon S, Batchelor B, Abdel-Wahab A (2013). Photochemical degradation of vinyl chloride with an advanced reduction process (ARP): Effects of reagents and pH. Chemical Engineering Journal, 215-216: 868–875

Liu Z, Bentel M J, Yu Y, Ren C, Gao J, Pulikkal V F, Sun M, Men Y, Liu J (2021). Near-quantitative defluorination of perfluorinated and fluorotelomer carboxylates and sulfonates with integrated oxidation and reduction. Environmental Science & Technology, 55(10): 7052–7062

Li X, Li Z, Xing Z, Song Z, Ye B, Wang Z, Wu Q (2020). UV-LED/P25-based photocatalysis for effective degradation of isothiazolone biocide. Frontiers of Environmental Science & Engineering, 15(5): 85

Li W, Ding Y, Sui Q, Lu S, Qiu Z, Lin K (2012). Identification and ecotoxicity assessment of intermediates generated during the degradation of clofibric acid by advanced oxidation processes. Frontiers of Environmental Science & Engineering, 6(4): 445–454

Meunier S M, Todorovic B, Dare E V, Begum A, Guillemette S, Wenger A, Saxena P, Campbell J L, Sasges M, Aucoin M G (2016). Impact of dissolved oxygen during UV-irradiation on the chemical composition and function of CHO cell culture media. PLoS One, 11(3): e0150957

Moradi M, Moussavi G (2018). Investigation of chemical-less UVC/VUV process for advanced oxidation of sulfamethoxazole in aqueous solutions: Evaluation of operational variables and degradation mechanism. Separation and Purification Technology, 190: 90–99

Moussavi G, Rezaei M (2017). Exploring the advanced oxidation/reduction processes in the VUV photoreactor for dechlorination and mineralization of trichloroacetic acid: Parametric experiments, degradation pathway and bioassessment. Chemical Engineering Journal, 328: 331–342

Motohashi N, Saito Y (1993). Competitive measurement of rate constants for hydroxyl radical reactions using radiolytic hydroxylation of benzoate. Chemical & Pharmaceutical Bulletin, 41(10): 1842–1845

Nosaka Y, Nosaka A Y (2017). Generation and detection of reactive oxygen species in photocatalysis. Chemical Reviews, 117(17):

11302–11336

Park H, Vecitis C D, Cheng J, Dalleska N F, Mader B T, Hoffmann M R (2011). Reductive degradation of perfluoroalkyl compounds with aquated electrons generated from iodide photolysis at 254 nm. Photochemical & Photobiological Sciences: Official journal of the European Photochemistry Association and the European Society for Photobiology, 10(12): 1945–1953

Pourakbar M, Moussavi G, Shekoohiyan S (2016). Homogenous VUV advanced oxidation process for enhanced degradation and mineralization of antibiotics in contaminated water. Ecotoxicology and Environmental Safety, 125: 72–77

Qu Y, Zhang C, Li F, Chen J, Zhou Q (2010). Photo-reductive defluorination of perfluorooctanoic acid in water. Water Research, 44(9): 2939–2947

Roth O, LaVerne J A (2011). Effect of pH on H_2O_2 production in the radiolysis of water. The Journal of Physical Chemistry A, 115(5): 700–708

Scott B F, Spencer C, Marvin C H, MacTavish D C, Muir D C G (2002). Distribution of haloacetic acids in the water columns of the Laurentian Great Lakes and Lake Malawi. Environmental Science & Technology, 36(9): 1893–1898

Song M, Wang J, Chen B, Wang L (2017). A Facile, nonreactive hydrogen peroxide (H_2O_2) detection method enabled by ion chromatography with UV detector. Analytical Chemistry, 89(21): 11537–11544

Sun Z, Zhang C, Chen P, Zhou Q, Hoffmann M R (2017a). Impact of humic acid on the photoreductive degradation of perfluorooctane sulfonate (PFOS) by UV/Iodide process. Water Research, 127: 50–58

Sun Z, Zhang C, Zhao X, Chen J, Zhou Q (2017b). Efficient photoreductive decomposition of N-nitrosodimethylamine by UV/iodide process. Journal of Hazardous Materials, 329: 185–192

Tobien T, Cooper W J, Asmus K D (2000). Natural organic matter and disinfection by-products. Washington, DC: American Chemical Society

Vicente J, Arcas A, Bautista D, Shul'pin G B (1994). Aerobic photooxidation and C–C bond cleavage of the acetylacetonate ligand in (2-arylazo)arylpalladium(II) complexes induced by visible light. Journal of the Chemical Society, Dalton Transactions: Inorganic Chemistry, 10: 1505–1509

Wang L, Niu R, Chen B, Wang L, Zhang G (2017). A comparison of photodegradation kinetics, mechanisms, and products between chlorinated and brominated/iodinated haloacetic acids in water. Chemical Engineering Journal, 330: 1326–1333

Wang L, Zhang Q, Chen B, Bu Y, Chen Y, Ma J, Rosario-Ortiz F L, Zhu R (2020). Some issues limiting photo(cata)lysis application in water pollutant control: A critical review from chemistry perspectives. Water Research, 174: 115605

Wang W L, Wu Q Y, Huang N, Wang T, Hu H Y (2016). Synergistic effect between UV and chlorine (UV/chlorine) on the degradation of carbamazepine: Influence factors and radical species. Water Research, 98: 190–198

Wei Y J, Liu C G, Mo L P (2005). Ultraviolet absorption spectra of iodine, iodide ion and triiodide ion. Spectroscopy and Spectral Analysis , 25(1): 86–88

Xie B H, Shan C, Xu Z, Li X C, Zhang X L, Chen J J, Pan B C (2017). One-step removal of Cr(VI) at alkaline pH by UV/sulfite process: Reduction to Cr(III) and in situ Cr(III) precipitation. Chemical Engineering Journal, 308: 791–797

Yang L, Li M, Li W, Bolton J R, Qiang Z (2018a). A green method to determine VUV (185 nm) fluence rate based on hydrogen peroxide production in aqueous solution. Photochemistry and Photobiology, 94(4): 821–824

Yang M, Jonsson M (2014). Evaluation of the O_2 and pH effects on probes for surface bound hydroxyl radicals. Journal of Physical Chemistry C, 118(15): 7971–7979

Yang X Y, Wei H, Xie J C, Wang N, Wei N, Wang J W (2018b). 4th International Conference on Water Resource and Environment. Kaohsiung City, July 17th to 21st, 2018

Yang C, Sun W, Ao X (2019). Bacterial inactivation, DNA damage, and faster ATP degradation induced by ultraviolet disinfection. Frontiers of Environmental Science & Engineering, 14(1): 13

Yeo J, Choi W (2009). Iodide-mediated photooxidation of arsenite under 254 nm irradiation. Environmental Science & Technology, 43(10): 3784–3788

Yu K, Li X, Chen L, Fang J, Chen H, Li Q, Chi N, Ma J (2018). Mechanism and efficiency of contaminant reduction by hydrated electron in the sulfite/iodide/UV process. Water Research, 129: 357–364

Zhang Q, Wang L, Chen B, Chen Y, Ma J (2020). Understanding and modeling the formation and transformation of hydrogen peroxide in water irradiated by 254 nm ultraviolet (UV) and 185 nm vacuum UV (VUV): Effects of pH and oxygen. Chemosphere, 244: 125483

Zhang T Y, Lin Y L, Wang A Q, Tian F X, Xu B, Xia S J, Gao N Y (2016). Formation of iodinated trihalomethanes during UV/chloramination with iodate as the iodine source. Water Research, 98: 199–205

Zoschke K, Börnick H, Worch E (2014). Vacuum-UV radiation at 185 nm in water treatment: A review. Water Research, 52: 131–145